Characterization of open and closed volcanic systems in Indonesia and Mexico using InSAR time series

E. Chaussard,[1,2] F. Amelung,[1] and Y. Aoki[3]

Received 25 March 2013; revised 8 July 2013; accepted 11 July 2013.

[1] We use 2007–2011 Advanced Land Observing Satellite (ALOS) data to perform an arc-wide interferometric synthetic aperture radar (InSAR) time series survey of the Trans-Mexican Volcanic Belt (TMVB) and to study time-dependent ground deformation of four Indonesian volcanoes selected following the 2007–2009 study of Chaussard and Amelung (2012). Our objectives are to examine whether arc volcanoes exhibit long-term edifice-wide cyclic deformation patterns that can be used to characterize open and closed volcanic systems and to better constrain in which cases precursory inflation is expected. We reveal deformation cycles at both regularly active and previously inactive Indonesian volcanoes, but we do not detect deformation in the TMVB, reflecting a lower activity level. We identify three types of relationships between deformation and activity: inflation prior to eruption and associated with or followed by deflation (Kerinci and Sinabung), inflation without eruption and followed by slow deflation (Agung), and eruption without precursory deformation (Merapi, Colima, and Popocatépetl; at Merapi, no significant deformation is detected even during eruption). The first two cases correspond to closed volcanic systems and suggest that the traditional model of magmatic systems and eruptive cycles do apply to andesitic volcanoes (i.e., inflation and deflation episodes associated with magma accumulation or volatile exsolution in a crustal reservoir followed by eruptions or in situ cooling). In contrast, the last case corresponds to open volcanic systems where no significant pressurization of the magmatic reservoirs is taking place prior to eruptions and thus no long-term edifice-wide ground deformation can be detected. We discuss these results in terms of InSAR's potential for forecasting volcanic unrest.

Citation: Chaussard, E., F. Amelung, and Y. Aoki (2013), Characterization of open and closed volcanic systems in Indonesia and Mexico using InSAR time series, *J. Geophys. Res. Solid Earth*, *118*, doi:10.1002/jgrb.50288.

1. Introduction

[2] The traditional model of a magmatic system assumes that overpressure in a magma reservoir, due to volatile exsolution or influx of new magma, eventually opens a conduit to the surface causing an eruption. Subsequent drainage of magma and gas from the reservoir releases overpressure and terminates the eruption. This model leads to the concept of the eruptive cycle [e.g., *Blake*, 1981; *Tait et al*., 1989; *Bower and Woods*, 1998; *Lu et al*., 2002; *Dzurisin*, 2003] suggesting that eruptions should be preceded by a pressure increase within the magma reservoir that is sufficiently large to cause fracturing of the reservoir wall and conduit formation or dike propagation. In this perspective, measurement of edifice-wide ground deformation due to reservoir pressurization can be used as an indicator for impending eruptive activity.

[3] Such cyclic, long-term, edifice-wide deformations corresponding to inflation-eruption-deflation patterns (with periods of months to years) have been mostly described at basaltic volcanoes [*Lu et al*., 2003; 2005; *Baker and Amelung*, 2012; *Toombs and Wadge*, 2012]. This type of behavior is in contrast to cyclic and acyclic short-term deformation of the summit area (with periods of hours to weeks) related to magma ascent in conduits observed at more silicic volcanoes [e.g., *Denlinger and Hoblitt*, 1999; *Voight et al*., 1999; *Nishimura*, 2009; *Surono et al*., 2012]. However, it is not clear to what extent silicic arc volcanoes exhibit long-term, edifice-wide deformation cycles. The lack of such observations may be due to the limitations of previous studies, which focused on individual volcanoes [e.g., *Froger et al*., 2007; *Riddick and Schmidt*, 2011; *Wicks et al*., 2011] and used interferograms instead of time series, suffering temporal aliasing [e.g., *Pritchard and Simons*, 2004; *Lu et al*., 2007; *Fournier et al*., 2010].

[4] *Chaussard and Amelung* [2012] conducted an interferometric synthetic aperture radar (InSAR) time series survey

Additional supporting information may be found in the online version of this article.

[1]Rosenstiel School of Marine and Atmospheric Science, University of Miami, Miami, Florida, USA.
[2]Now at the Department of Earth and Planetary Science, University of California, Berkeley, California, USA.
[3]Earthquake Research Institute, University of Tokyo, Tokyo, Japan.

Corresponding author: E. Chaussard, Department of Earth and Planetary Science, 382 McCone Hall, University of California Berkeley, Berkeley, CA 94720-4764, USA. (estelle@seismo.berkeley.edu)

2169-9313/13/10.1002/jgrb.50288

of the west Sunda volcanic arc and detected inflation at six volcanoes, three of which erupted afterwards, suggesting that the traditional model of magmatic systems may also apply to silicic volcanoes. However, they could not constrain cyclic deformation because they studied only a 2 year period.

[5] To better understand the relationships between deformation and volcanic activity, we first conduct an arc-wide ground deformation survey of the Trans-Mexican Volcanic Belt (TMVB) using 2007–2011 Advanced Land Observing Satellite (ALOS) InSAR (the satellite suffered power failure in April 2011). Because the TMVB is located in extensional tectonic setting [e.g., *Garcia-Palomo et al*., 2000], we expect magma reservoirs (storage zones of partially molten bodies, sometimes referred to as magma chambers [e.g., *Gudmundsson*, 2012]) to be located at shallow depths [*Chaussard and Amelung*, 2012]. Some shallow reservoirs have already been documented [*Straub and Martin-Del Pozzo*, 2001; *Zobin et al*., 2002]. Deformation resulting from pressurization of such reservoirs is readily detected by InSAR [e.g., *Biggs et al*., 2009]. Second, we use the 2007–2011 InSAR time series to test for cyclic deformation at four volcanoes of the west Sunda arc, selected according to the results of the 2007–2009 survey of *Chaussard and Amelung* [2012] (only four volcanoes are studied because of changes in the Japanese Space Exploration Agency's data distribution policy). We selected volcanoes with a wide spectrum of deformation behavior: Sinabung and Kerinci in Sumatra, which inflated and erupted; Agung in Bali, which inflated but did not erupt; and Merapi in Java, which erupted but no deformation was previously detected.

[6] Throughout this paper we refer to *closed volcanic systems* as volcanoes with sealed conduits that may exhibit edifice-wide long-term ground uplift due to reservoir pressurization. They are in contrast to *open volcanic systems* with permanent or semipermanent open conduits that may show short-term, localized deformation related to conduit processes but do not experience significant reservoir pressurization.

[7] This paper is organized as follows: First, we present the background geological information. Second, we summarize the data used and the analysis methods. Third, we present the results of the TMVB survey followed by the observations at the west Sunda volcanoes. Fourth, we compare the results obtained in the two arcs and discuss the observed relationships between deformation and activity, and implications for the magmatic systems. Lastly, we investigate the potential and limitations of InSAR observations for forecasting volcanic unrest.

2. Tectonic and Volcanic Settings of the Studied Arcs

2.1. The Trans-Mexican Volcanic Belt

[8] The Trans-Mexican Volcanic Belt, in central Mexico, results from the subduction of the Cocos Plate under the North American Plate at ~55 mm/yr [*Ferrari et al*., 2012; *Ramírez-Herrera and Urrutia-Fucugauchi*, 1999]. The arc is composed of 20 polygenetic andesitic to dacitic stratovolcanoes, 11 of which have been historically active [*Simkin and Siebert*, 2002]. The explosive, often Plinian eruptions of these volcanoes threaten millions of people living in their vicinity [e.g., *Davila et al*., 2007; *Zobin et al*., 2009]. For example, Popocatépetl is located only 70 km southeast of the capital Mexico City (21.2 million people) and 40 km west of the major city of Puebla (2.7 million people). In addition, volcanism also occurs in extensive monogenetic provinces, such as the Michoacán-Guanajuato volcanic field, home of ~1400 volcanoes, including the historically active Parícutin (1943–1952) and Jorullo (1759–1774) cinder cones.

[9] During the past century, only three polygenetic volcanoes of the TMVB experienced eruptions: Colima, Popocatépet, and El Chichón (from west to east). El Chichón last erupted in 1982, while Colima and Popocatépetl have both been regularly active in the past 20 years and experienced unrest during our survey period.

[10] Colima is Mexico's historically most active volcano with over 40 eruptions since the sixteenth century. Its last Plinian eruption in 1913 left a deep summit crater that was slowly refilled [*Simkin and Siebert*, 2002]. Colima's 2007–2011 unrest was dominated by lava dome growth in the crater [*Zobin et al*., 2006; *James and Varley*, 2012].

[11] Popocatépetl, in the eastern half of the TMVB, had several major eruptions in the last 5000 years including three Plinian events, the latest of which took place in 800 A.D. [*Simkin and Siebert*, 2002]. Most of its eruptions in the past 600 years were relatively small. Its 2005–2011 unrest period was characterized by dome growth and destruction, ash plumes, gas-and-steam emissions, and explosions [*De La Cruz-Reyna et al*., 2008].

2.2. The West Sunda Volcanic Arc

[12] The Indonesian arc, home of 13% of the world's active volcanoes, results from the subduction of the Australian Plate under the Sunda Plate at rates varying from 47 mm/yr in North Sumatra, to 72 mm/yr in Java [*McCaffrey*, 2009]. The western portion of the arc, the west Sunda arc, is composed of 84 andesitic to dacitic stratovolcanoes in Sumatra, Java, and Bali, 76 of which have been historically active [*Simkin and Siebert*, 2002]. Because several millions of people live in the proximity of these frequently erupting, explosive volcanoes, the Indonesian arc is responsible for 67% of the worldwide volcano-related fatalities [*Blong*, 1984; *Simkin and Siebert*, 2002]. Below we present the recent activity history of the four west Sunda volcanoes studied in detail.

[13] Sinabung, in northern Sumatra, had no recorded historical eruptions prior to its reawakening in August 2010 [*Simkin and Siebert*, 2002]. This Vulcanian eruption was characterized by 5–6 km high ash plumes and lava effusion and resulted in the evacuation of 12,000 people. On September 30, a month after the start of unrest, activity decreased to minor degassing near the crater [*Simkin and Siebert*, 2002].

[14] Kerinci, in central Sumatra, has had more than 25 moderately explosive eruptions since its first recorded in 1838, including seven since 1990 [*Simkin and Siebert*, 2002]. Its latest eruptions occurred on 9 September 2007, at the end of March 2008, and from 1 April to 19 June 2009. Unrests in 2007 and 2008 were characterized by small gas plumes, while the 2009 eruption was more vigorous with ash and gas plumes that rose 500–1000 m above the vent and explosions that ejected ballistic material.

[15] Agung, in Bali, last erupted in 1963–1964 after a century of inactivity [*Simkin and Siebert*, 2002]. This eruption resulted in 1100 fatalities and was Indonesia's largest and most devastating eruption of the twentieth century, which also influenced the Earth's climate [*Self and Rampino*,

Table 1. ALOS PALSAR Scenes Processed to Study the TMVB and the Four West Sunda Volcanoes[a]

Track	Frame	Earliest Scene	Latest Scene	Number of scenes	Number of interferograms	Volcano(es)
			Trans-Mexican Volcanic Belt			
179	350–360	2-Mar-07	13-Mar-11	12	21	San Martin
181	380	18-Feb-07	14-Jan-11	12	24	Los Atlixcos, Naolinco Volcanic Field
183	360–370	6-Feb-07	2-Jan-11	11	16	Cofre de Perote, La Gloria, Serdan-Oriental, Las Cumbres, Pico de Orizaba
184	370	26-Aug-07	19-Jan-11	13	27	La Malinche
185	370	28-Jul-07	21-Dec-10	11	21	Papayo, Iztaccihuatl, *Popocatepetl*
186	370	11-Feb-07	7-Jan-11	19	47	Chichinautzin, Ajusco
187	370–380	28-Feb-07	9-Dec-10	13	26	Jocotitlan, Ajusco, Nevado de Toluca
188	370–400	2-Aug-07	10-Jan-11	14	28	Zitácuaro-Valle de Bravo, Nevado de Toluca
189	380–390	19-Aug-07	27-Feb-11	15	41	Michoacán-Guanajuato field
190	380–400	5-Mar-07	16-Mar-11	18	40	Michoacán-Guanajuato field
191	380–390	7-Aug-07	15-Feb-11	17	42	Michoacán-Guanajuato field
192	380–390	24-Aug-07	4-Mar-11	16	31	Michoacán-Guanajuato field (Paricutin)
194	380	12-Aug-07	20-Feb-11	14	18	Nevado de Colima
195	370 and 410	26-Feb-07	9-Mar-11	13	27	Nevado de Colima, *Colima*
196	410	30-Apr-07	24-Dec-10	13	28	Ceboruco, Sanganguey
			West Sunda Arc			
422	7010	21-Feb-07	4-Mar-11	26	73	Agung, Batur
431	7030	8-Jun-07	1-Feb-11	23	73	*Merapi*, Merbabu, Telomoyo
446	7150	3-Jul-07	26-Nov-10	21	54	*Kerinci*
495	50	20-Feb-07	16-Jan-11	21	55	*Sinabung*, Sibayak

[a]The volcanoes covered by each track are shown in the last column; the ones with unrest periods during the survey time are in italics.

2012; *Hansen et al*., 1978]. This subPlinian eruption had two paroxysmal explosive phases (volcanic explosivity index (VEI) 5) and generated widespread ash fall and pyroclastic flows leading to lahars that destroyed many villages.

[16] Merapi, located north of Central Java's capital Yogyakarta, is Indonesia's most active volcano. It erupts every 5–10 years and produces Plinian eruptions every century [*Surono et al*., 2012]. Merapi had three unrest periods during our observation time: in 2007, 2008, and 2010. The first two were characterized by periodic lava dome growth, similar to Popocatépetl and Colima [*Simkin and Siebert*, 2002], while the last one, defined as the century eruption, produced pyroclastic flows, ash plumes, and explosions between 26 October and 2 November 2010. This eruption resulted in the death of 400 people and the evacuation of ~400,000 [*Surono et al*., 2012; *Pallister et al*., 2012].

3. Data and Method

3.1. InSAR Data and Method

[17] InSAR has been demonstrated to be a useful tool to measure surface deformation associated with multiple geohazards: earthquakes, volcanic eruptions, and anthropogenic activities [e.g., *Massonnet et al*., 1993; *Amelung et al*., 2000; *Chaussard et al*., 2013]. Ground displacement in the radar line-of-sight (LOS) direction is obtained from the phase difference of synthetic aperture radar (SAR) pairs of the same area acquired at different times (interferograms). We use a modified version of the Gamma software to process Single Look Complex images and the ROI_PAC software developed at NASA's Jet Propulsion Laboratory [*Rosen et al*., 2004] to produce interferograms.

[18] To survey 90,000 km^2 in the TMVB, we used 450 ALOS images acquired between 2007 and 2011 and produced ~2200 interferograms. Table 1 summarizes the data used. For the west Sunda arc, we focused on four volcanoes (Sinabung, Kerinci, Agung, and Merapi) adding 2 years of ALOS data and 255 interferograms to the data discussed by *Chaussard and Amelung* [2012].

3.2. InSAR Time Series Analysis

[19] We use the small baseline subset (SBAS) method [*Berardino et al*., 2002; *Lanari et al*., 2004] to obtain displacement time series from the InSAR data. In this method a network of interferograms is inverted to retrieve the surface displacement through time. We select the interferogram network using the following approach. We first use a Delaunay triangulation to obtain an interconnected network of interferometric pairs (Figure 1, all lines). We then select

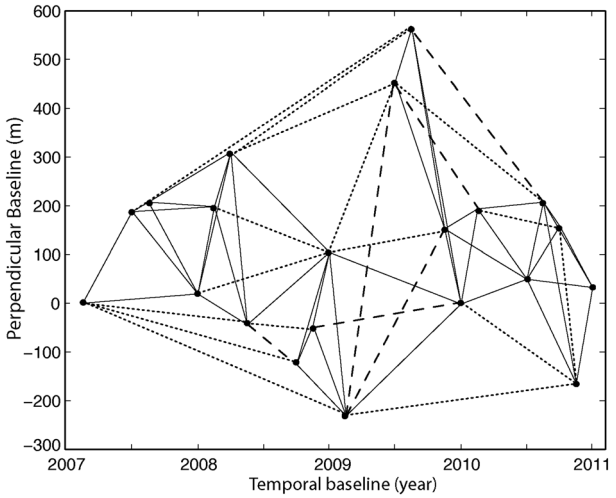

Figure 1. Perpendicular baseline-time plot of a triangulated network of interferometric pairs for Sinabung. All lines: Delaunay triangulation. Solid lines: pairs used for the time series inversion. Dotted lines: pairs with perpendicular and temporal baselines above the selected threshold (1.5 km and 1 year). Dashed lines: pairs with low coherence.

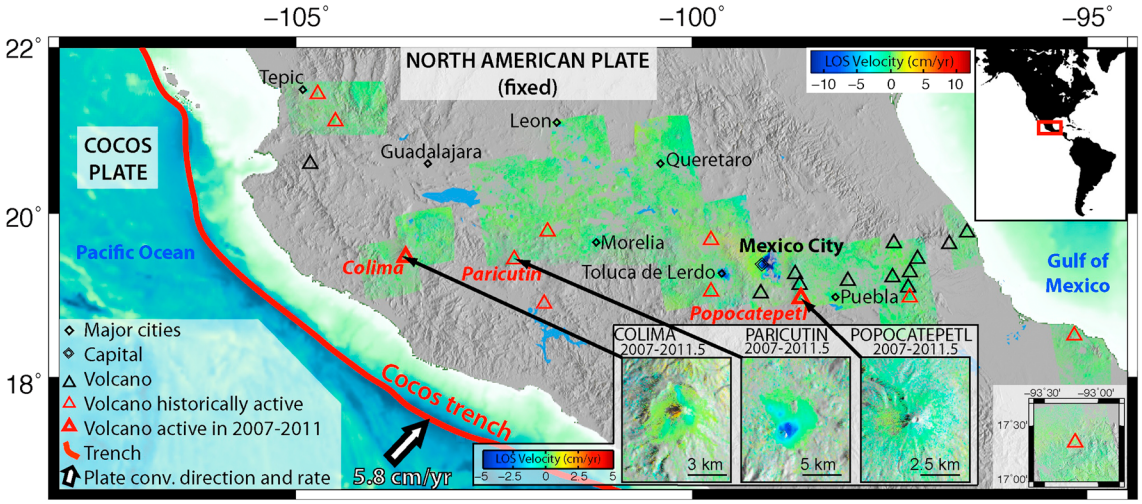

Figure 2. Averaged 2007–2011 LOS velocity map of the Trans-Mexican Volcanic Belt, from ALOS InSAR. Only pixels with a temporal coherence larger than 0.7 are shown. Red triangles: historically active volcanoes (bold: those active during the survey period). Black triangles: other volcanoes. Black diamonds: major cities near volcanoes. White arrow: relative plate convergence rate at the Cocos Trench. Positive LOS velocities (uplift) are shown in red and negative LOS velocities (subsidence) in blue. Labeled insets: zoomed in for volcanoes showing deformation (Parícutin) or volcanoes active during the time period of the survey (Colima and Popocatépetl). These insets have a smaller color scale. Bottom right inset: LOS velocity map of El Chichón, volcano located southeast of the area shown.

interferograms with small spatial (<1.5 km) and small temporal (<1 year) baselines to maintain high coherence (Figure 1, removing dotted line pairs). Finally, we examine each interferogram and remove those with low coherence on the volcanoes (Figure 1, removing dashed line pairs). If the remaining network is not fully connected, we add interferograms with larger baselines but good coherence.

[20] This semiautomatic approach is an effort to achieve a balance between using only interferograms with good coherence in the areas of interest and maintaining a fully connected network (describing an overdetermined problem). It is practical for ALOS InSAR because of the relatively small number of acquisitions available for each frame (less than 30). An alternative method is the automated approach of *Baker and Amelung* [2012], in which interferograms are selected using a threshold for the percentage of pixels within an area of interest above a given coherence. However, the appropriate threshold depends on the interferogram quality and the size and location of the area of interest, which still involves manual evaluation of the interferograms.

[21] The SBAS method allows one to obtain the displacement between any two acquisitions, regardless of the possibility of generating a particular interferogram. We reference the displacement time series to a single pixel that exhibits high coherence and is located far enough from the volcanoes to not be affected by significant deformation. We apply a temporal coherence threshold to the final time series, calculated using the formulation by *Tizzani et al.* [2007] and *Gourmelen et al.* [2010] to eliminate bias from phase-unwrapping errors. We select only pixels with a temporal coherence greater than 0.7, a typical value in InSAR applications [*Casu et al.*, 2006; *Tizzani et al.*, 2007]. We correct for digital elevation model (DEM) errors after the time series inversion by identifying and removing the dependency of the displacement history to the perpendicular baseline history [*Fattahi and Amelung*, 2013] (example shown in Figure S1 in the supporting information).

3.3. Atmospheric Noise

[22] Atmospheric phase delays can be decomposed into two sources, the layered atmosphere (differences in temperature, pressure, and water content at different elevations) and the turbulent atmosphere (variable water vapor distribution) [*Zebker et al.*, 1997; *Emardson et al.*, 2003]. The two commonly used methods to mitigate atmospheric delays rely on global meteorological models [*Jolivet et al.*, 2011] or spatial-temporal filtering [*Colesanti et al.*, 2003].

[23] Here we use the following strategy. We first eliminate acquisitions potentially affected by strong atmospheric noise: we isolate outliers from a trend in the time series and use pairwise logic on the original interferograms (which have more coherent pixels than the time series) to confirm that a particular acquisition is affected by atmospheric delays (example in Figure S2).We then identify atmospheric delays by comparing the range change measurements at a volcano of interest with the ones at a neighboring inactive volcano of similar elevation. If the measurements at the two volcanoes correlate, they reflect atmospheric phase delay rather than ground deformation. Correlated delays can be due to the layered or the turbulent atmosphere since turbulent effects are stronger in areas with significant topography.

4. Results

[24] First, we present the results for the TMVB and west Sunda arc in form of averaged LOS velocity maps (Figures 2 and 3, ground motions toward and away from the satellite being shown with red and blue colors, respectively). These maps allow the identification of actively deforming volcanoes related to subsurface magma movements or hydrothermal

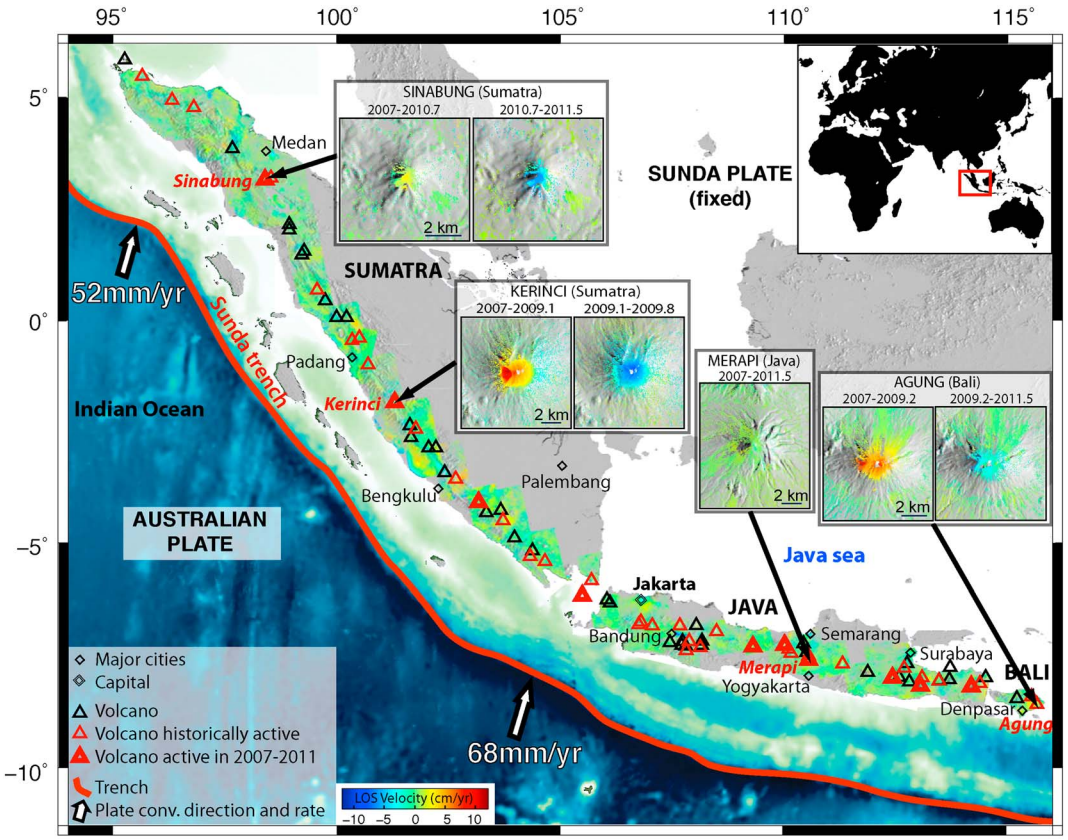

Figure 3. Averaged 2007–2009 LOS velocity map of the west Sunda arc, Indonesia, from ALOS InSAR (see Figure 2 for legend). Data of *Chaussard and Amelung* [2012] supplemented by imagery through 2011 for Sinabung, Kerinci, Merapi, and Agung volcanoes. Insets show averaged LOS velocity maps at these volcanoes for activity periods described in the text.

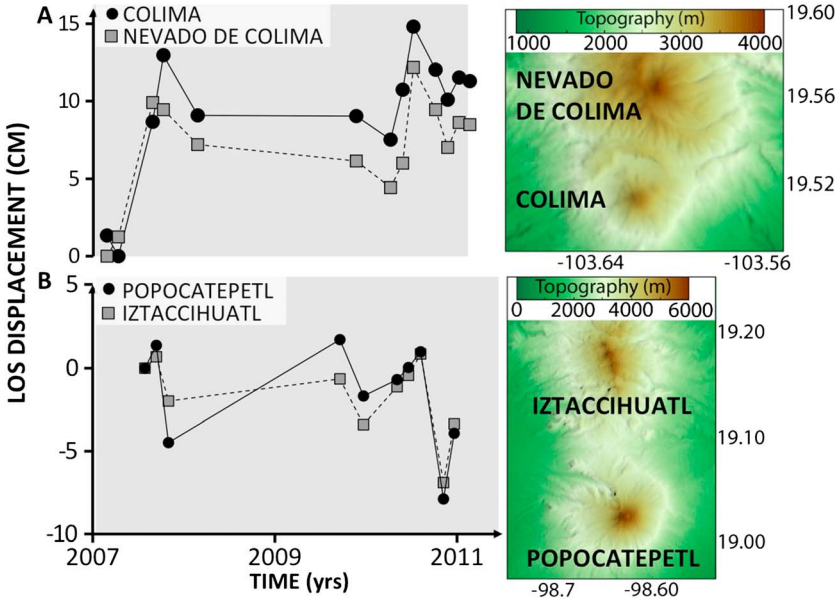

Figure 4. LOS displacement time series near the summits of (a) Colima and (b) Popocatépetl volcanoes (black circles) and for inactive neighboring volcanoes (Nevado de Colima and Iztaccíhuatl, respectively, grey squares). Grey shaded area: activity period (continuous in both cases). The DEMs on the right show the locations of the volcanoes.

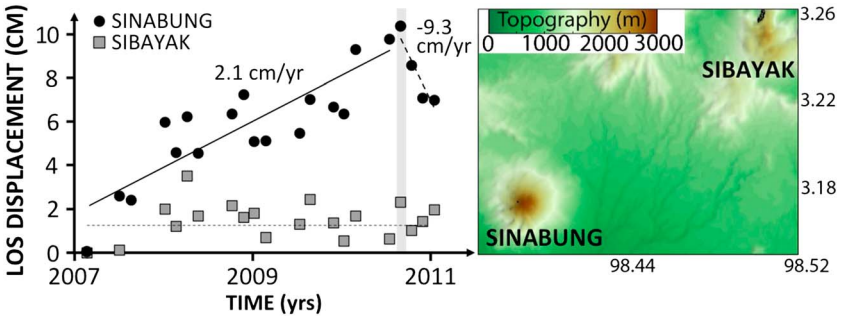

Figure 5. Same as Figure 4 but for Sinabung (black circles) and its inactive neighbor Sibayak (grey squares). Black lines: best fitting linear regressions for the different periods of activity with the corresponding deformation rates. Full line: well-constrained deformation trend; dashed line: possible deformation trend, the temporal pattern being poorly constrained. Grey shaded area shows activity periods.

effects. Second, we present LOS displacement time series near the summit of the selected volcanoes, which represent either ground motion or atmospheric delays (Figures 4–8). Positive LOS displacements represent motion toward the satellite (i.e., uplift in case of ground deformation) and negative LOS displacements motion away from the satellite (subsidence). In highly variable time series, results from successive SAR acquisitions are connected by a line (Figures 4 and 8), whereas for time series with a clear trend, the best fitting linear regressions are shown (Figures 5, 6, and 7). The SAR dates are in decimal years rounded to the first decimal; this is a unique identifier because the shortest time span between two ALOS acquisitions is 0.13 years (46 days).

4.1. Mexico

[25] The InSAR survey of the TMVB did not reveal substantial inflation at any of the 20 volcanic edifices (Figure 2). The most notable signals are subsidence in Mexico City and Toluca [*Cabral-Cano et al.*, 2008; *Osmanoglu et al.*, 2011] (E. Chaussard et al., Land subsidence in central Mexico detected by ALOS InSAR time-series, submitted to *Remote Sensing of Environment*, 2013) (Figure 2). The measurement noise of the averaged LOS velocity map is ~2 cm/yr (green-yellow colors) and varies along the arc depending on the number of SAR acquisitions and the atmospheric conditions. The only clear signal associated with a volcano is subsidence in the lava field of Parícutin, a monogenetic volcano of the Michoacán-Guanajuato volcanic field (also observed by *Fournier et al.* [2010]) (Figure 2, central inset). No clear deformation is detected at the three historically active volcanoes (El Chichón, Popocatépetl, and Colima). In the following three sections we describe the results for the latter two, which experienced unrest during our observation time.

4.1.1. Colima

[26] Thirteen SAR images covering Colima were acquired between early 2007 and early 2011. The LOS displacement time series near the summit is highly variable (Figure 4a, black circles) and could represent either successive uplift periods or atmospheric effects. To evaluate the atmospheric contributions, we compare this time series with the one at Nevado de Colima (Figure 4a, grey squares), the neighboring inactive volcano 5 km to the north and with a similar elevation (3850 and 4320 m for Colima and Nevado de Colima, respectively). The similarity of the time series indicates that the LOS displacements are caused by atmospheric phase delays rather than ground deformation.

4.1.2. Popocatépetl

[27] Eleven SAR images covering Popocatépetl were acquired between mid-2007 and the end of 2010. Similar to the case of Colima, the LOS displacement time series is highly variable (Figure 4b, black circles). The time series at Popocatépetl and at its neighboring inactive volcano Iztaccíhuatl, 15 km to the north and with a similar elevation (5426 and 5230 m, Figure 4b, black circles and grey squares, respectively), are correlated, suggesting that the LOS displacements are caused by atmospheric phase delays.

4.2. West Sunda

[28] Ground velocity maps at Sinabung, Kerinci, Agung, and Merapi covering the 2007–2011 time period are shown in Figure 3 (insets). We detect inflation followed by deflation at three volcanoes: Sinabung and Kerinci in Sumatra and Agung in Bali, while no clear deformation is observed at Merapi in Java.

4.2.1. Sinabung

[29] Twenty-one SAR images covering Sinabung were acquired between early 2007 and early 2011. The time series shows ~10 cm of LOS displacement toward the satellite between 2007.1 and 2010.7 and 3 cm of LOS displacement away from the satellite after 2010.7, following the September 2010 eruption (Figure 5, black circles). The time series of Sibayak, the neighboring inactive volcano located 15 km northeast and with a similar elevation (2212 versus 2460 m for Sinabung, Figure 5, grey squares), is nearly flat,

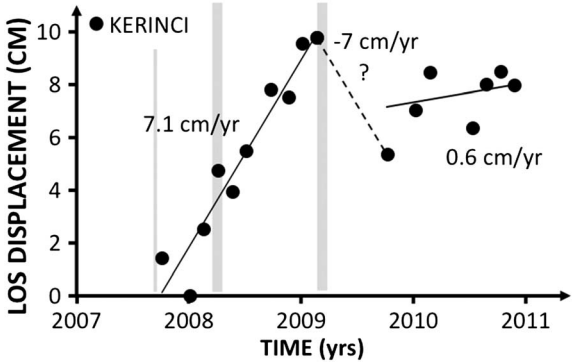

Figure 6. Same as Figure 5 but for Kerinci Volcano.

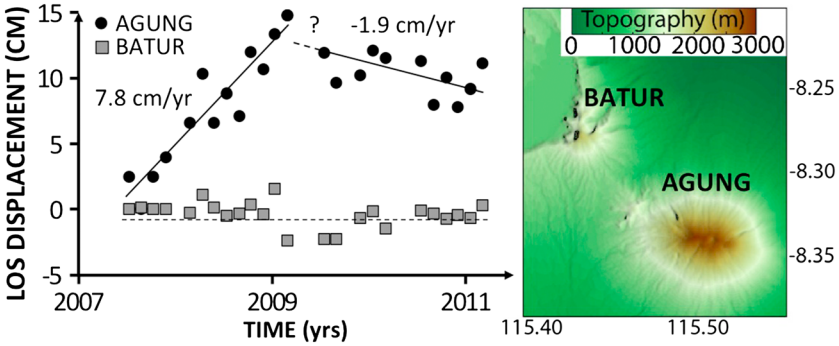

Figure 7. Same as Figure 5 but for Agung (black circles) and its inactive neighbor Batur (grey squares).

confirming that the LOS displacements at Sinabung represent real ground deformation.

[30] The time series suggests uplift at a rate of ~2 cm/yr prior to the 29 August 2010 eruption, in agreement with the 2007–2009 study of *Chaussard and Amelung* [2012], followed by rapid subsidence (Figure 5). However, as ALOS stopped operations in April 2011, we do not have enough observations to resolve the temporal sequence of deflation and whether it was coeruptive, instantaneous, or posteruptive and spread out over a longer time period. The net change between the last acquisition prior to the eruption (2010.5) and the first acquisition after the beginning of the eruption (31 August 2010, 2010.7) is uplift. It is possible that short-term preeruptive inflation masks deflation starting with the eruption or that the 2010.7 acquisition is affected by atmospheric delays. The three subsequent acquisitions suggest a posteruptive subsidence rate of ~9 cm/yr.

4.2.2. Kerinci

[31] Seventeen SAR images covering Kerinci were acquired between mid-2007 and the end of 2010. The time series shows ~10 cm of LOS displacement toward the satellite between 2007.8 and 2009.1 and 4 cm of LOS displacement away from the satellite during 2009.1–2009.8 associated with the April–June 2009 eruption (Figure 6). During 2009.8–2010.9, no significant LOS displacement is detected, most of the variance in the displacement time series being likely due to atmospheric delays, but no other volcano is present in the vicinity of Kerinci for comparison.

[32] The clear linear trend prior to the April–June 2009 eruption period suggests that the LOS displacements at Kerinci correspond to real ground deformation. At least 1 year of inflation at a linear rate of ~7 cm/yr is observed prior to the eruption, in agreement with previous observations [*Chaussard and Amelung*, 2012]. Because of the lack of acquisitions between February 2009 and October 2010, we are not able to constrain the deformation associated with and during the first 6 months after the eruption. However, it seems that the inflation period halted with the April–June 2009 eruption. The 4 cm of LOS subsidence between 2009.1 and 2009.8 reflects either linear subsidence at a rate of 7 cm/yr or sudden subsidence following the eruption. Because we do not consider significant the subtle inflation (at ~0.6 cm/yr) after October 2009, the subsidence period appears limited to the first 7 months following the eruption, and as of the end of 2010, the volcano remained close to its preeruption state.

4.2.3. Agung

[33] Twenty-three SAR images covering Agung were acquired between mid-2007 and mid-2011. The time series shows ~15 cm of LOS displacement toward the satellite between 2007.5 and 2009.2 and ~7 cm away from the satellite after 2009.2 (Figure 7, black circles). The time series at Batur, the neighboring inactive volcano located 18 km northwest (Figure 7, grey squares), is nearly flat, confirming that the LOS displacements at Agung represent real ground deformation.

[34] The time series reveals uplift at a linear rate of ~8 cm/yr prior to 2009.2, slightly higher than that reported by *Chaussard and Amelung* [2012] probably because of the additional data. Inflation at Agung stopped at 2009.2, and a period of slow subsidence started at a rate of ~2 cm/yr, despite the lack of eruption.

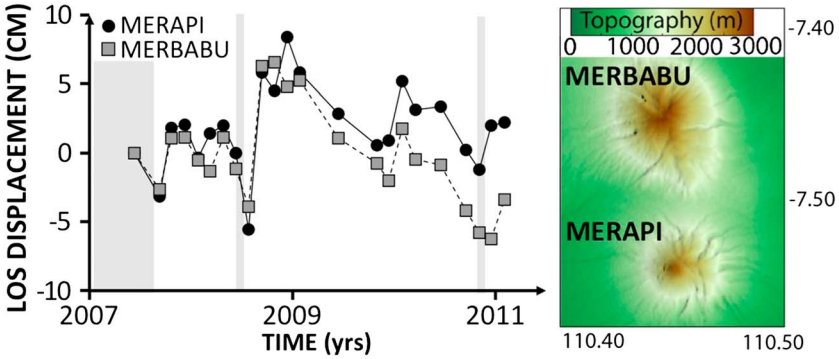

Figure 8. Same as Figure 5 but for Merapi Volcano (black circles) and its inactive neighbor Merbabu (grey squares).

4.2.4. Merapi

[35] Twenty-three SAR images covering Merapi were acquired between mid-2007 and early 2011. The LOS displacement time series near the summit is highly variable (Figure 8, black circles), similar to the ones described at Colima and Popocatépetl. The time series at Merapi and at its neighboring inactive volcano Merbabu, ~10 km to the north and with a similar elevation (2968 and 3145 m, Figure 8, black circles and grey squares, respectively), are correlated, suggesting that the LOS displacements are due to atmospheric phase delays, consistent with the results of *Chaussard and Amelung* [2012].

[36] Following the observation of a systematic and increasing offset between the time series at Merapi and Merbabu starting in 2009, we investigate the possibility of using Merbabu's time series to correct the atmospheric signal at Merapi and resolve subtle inflation prior to the October 2010 eruption (Figure S3). However, the signal obtained by differentiating the time series remains ambiguous and still likely dominated by atmospheric effects.

5. Discussion

5.1. Comparison Between the Two Volcanic Arcs

[37] The observation that none of the volcanoes of the TMVB are deforming is in contrast to observations in the west Sunda arc where *Chaussard and Amelung* [2012] identified inflation at six volcanoes and subsidence at one volcano during 2007–2009. We showed that at least three of these volcanoes continued to deform during 2009–2011. Although the TMVB has only one quarter as many volcanoes, this suggests that it is characterized by a much lower activity level than the west Sunda arc.

[38] This difference in the number of inflating volcanoes is consistent with differences in the reported historic activity and the activity over the last century. In the TMVB, only 11 out of the 20 volcanoes had historic activity and three in the last hundred years (55 and 15%, respectively) [*Simkin and Siebert*, 2002]. In contrast, in the west Sunda arc, 76 of the 84 volcanoes had historic activity and 60 in the last century (90 and 71%, respectively). These differences in the number of eruptions are consistent with the ~50 times lower magmatic output (eruptive rates) for the last thousand years or more of the Mexican volcanic arc compared to the Indonesian arc (1.37×10^{-4} versus 6.6×10^{-3} km^3) [*White et al*., 2006; *Vazquez and Reid*, 2004]. Thus, the lack of inflating volcanoes reflects the lower activity level of the TMVB rather than any other fundamental differences in the mode of magma ascent. However, the reason why the activity level is different is unknown. The west Sunda and Mexican arcs are in similar subduction setting (convergence rates of 4–7 cm/yr and slab dip angles of 30–40° below the arcs [*Hughes and Mahood*, 2011]), in similar tectonic settings (extension to strike-slip stress regimes) [*Chaussard and Amelung*, 2012], and on crusts with similar thicknesses (~30 km) [*Hughes and Mahood*, 2011].

5.2. Unrest and Precursory Deformation: Closed Versus Open Volcanic Systems

[39] We have identified three different types of relationships between deformation and volcanic activity: volcanoes that inflate prior to eruption (Sinabung and Kerinci), volcanoes that inflate but do not erupt (Agung), and volcanoes that erupt but do not show precursory deformation (Merapi, Colima, and Popocatépetl). Other significant observations include that (1) Sinabung did not erupt for centuries, whereas Kerinci is erupting every few years; (2) eruptions of both volcanoes were associated with or followed by subsidence (our observations do not allow us to constrain whether subsidence was coeruptive or posteruptive, as described above); (3) Agung's inflation was followed by slow subsidence despite the lack of any eruption; and (4) no significant deformation was observed even during eruption at Merapi. We now separately discuss volcanoes that show inflation (followed or not by an eruption) and volcanoes that do not.

[40] Here we refer with the terms open and closed volcanic systems to the part of the volcano between the shallowest reservoir and the surface. Closed volcanic systems correspond to volcanoes with sealed conduits, while open volcanic systems correspond to volcanoes with permanent or semipermanent open conduits. Open systems are characterized by frequent degassing (open vent [e.g., *Newhall*, 2007]) and lava dome growth (closed vent). Edifice-wide inflation can only occur at closed volcanic systems where the reservoir pressurization results in significant long-term ground uplift (months prior to eruption), in contrast to short-term deformation (days to weeks prior to eruption). At open volcanic systems, magma rises through the established conduit, resulting in limited pressurization of the reservoir and the absence of edifice-wide long-term inflation [*Albino et al.*, 2011]. Our use of these terms is in contrast to petrological studies in which they refer to the part of the volcanic system between a deep magma source and a shallower reservoir [e.g., *Zellmer et al*., 2005; *White et al*., 2006].

5.2.1. Inflating Volcanoes: Closed Systems

[41] The different activity stages at closed volcanic systems, with different expressions in terms of surface deformation, are summarized in a cartoon of the eruptive cycle model in Figure 9. When no magma is supplied from depth to the shallow magma system, the volcano is in repose in the sense that no surface deformation is occurring (Figure 9, stage a). Influx of new magma or exsolution of volatiles leads to the pressurization of the reservoir and inflation of the volcanic edifice (Figure 9, stage b). When the pressure exceeds the strength of the reservoir wall (i.e., exceeds the critical overpressure), the wall breaks, magma ascends through a conduit or dike toward the surface, and the volcano erupts (case 1 in Figure 9). The drainage of magma and gas from the reservoir is associated with pressure decrease and deflation of the edifice (Figure 9, stage c). After a repose period the cycle begins anew. An alternative scenario is that the pressure in the reservoir remains below the critical overpressure and no eruption occurs (case 2 in Figure 9). The shutdown of the magma influx leads to cooling and degassing of the magma in the reservoir, associated with slow deflation of the edifice (Figure 9, stage c′). Stages of this eruptive cycle have been previously described by *Blake* [1981] for eruptions driven by magma influx and by *Tait et al*. [1989] for eruptions driven by gas exsolution.

5.2.1.1. Inflation

[42] Periods of inflation at Sinabung, Kerinci, and Agung suggest that progressive magma recharge or gas exsolution leads to the pressurization of the magma reservoirs (Figure 9, stage b). Because our data start only in 2007, we

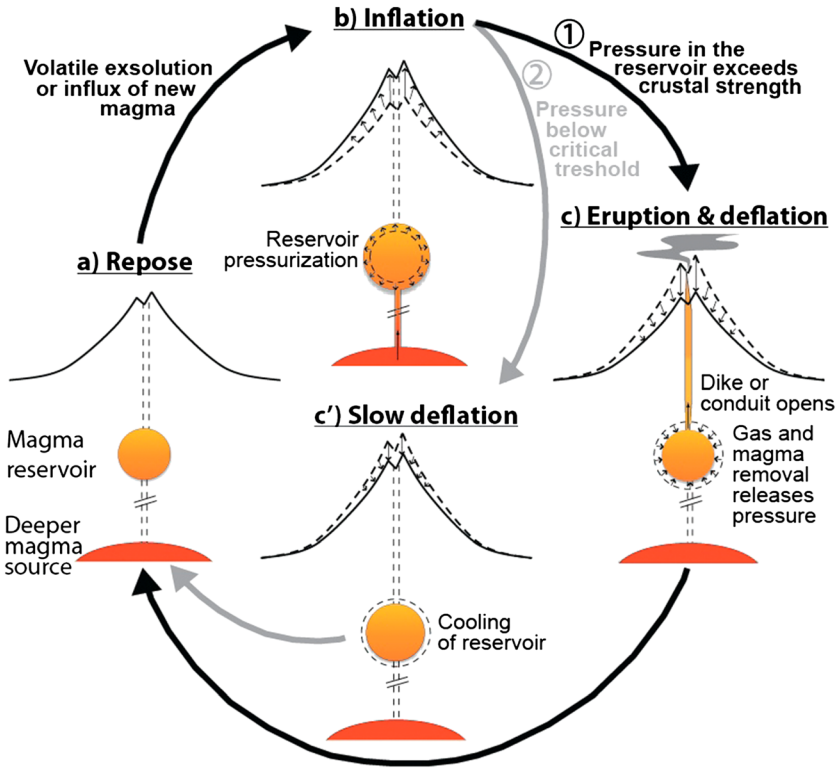

Figure 9. Cartoon for the eruptive cycle model of closed volcanic systems, consisting of repose (stage a), inflation (stage b), eruption and deflation (stage c), or no eruption and slow deflation (stage c′). Case 1: inflation followed by eruption (as seen at Kerinci and Sinabung). Case 2: inflation not followed by eruption (as seen at Agung), when the pressure in the reservoir remains below the critical overpressure.

are not able to constrain the end of the repose and start of the inflation period. At Sinabung, the long period of inactivity (centuries) suggests that the reservoir was cooled and depressurized. Thus, it is very likely that magma influx pressurized the system, resulting in the observed inflation, following the model of *Blake* [1981]. Kerinci erupts regularly (every few years), and its eruptions involve gas and ash plumes rather than massive lava flows. Because of the short repose time, the small size of the eruptions (VEI 1), and the limited amount of magma involved, we hypothesize that Kerinci's inflation was largely driven by gas exsolution rather than by influx of new magma, following the model of *Tait et al*. [1989]. Gravity change observations could distinguish between the two modes of inflation [e.g., *Battaglia et al*., 1999], but such measurements are not available. At all volcanoes, the observed inflation probably represents both instantaneous elastic deformation, contemporary with magma influx or gas exsolution, and delayed viscoelastic deformation for reservoirs surrounded by viscoelastic shells [e.g., *Dragoni and Magnanensi*, 1989].

[43] *Chaussard and Amelung* [2012] inferred from the geodetic observations that the reservoirs are small (radius ~1 km) and located at shallow depths (~1–3 km below the regional elevation, corresponding to less than 5 km below the summits). They did not invert for the sources' radii because of the well-known trade-offs in elastic modeling between the source's radius, overpressure, and depth. However, because the deformation pattern is confined to the volcanic edifices, only small and shallow magma reservoirs can explain the observations. New magma influx into such reservoirs likely leads to rapid pressure increase and eruption [*Jellinek and DePaolo*, 2003], consistent with the occurrence of eruptions at Sinabung and Kerinci. The fact that the inflation at Agung did not lead to eruption suggests that the pressure in the reservoir remained below the critical overpressure either because the volcano was originally far from a critical state [e.g., *Pinel et al*., 2010], possibly as a consequence of the massive 1963–1964 eruption (VEI 5) that could have emptied part of the reservoir, or because the reservoir is contained in country rocks with a lower effective viscosity [*Jellinek and DePaolo*, 2003]. Alternatively, the critical overpressure might have been reached, causing the reservoir to rupture, but some physical barrier prevented magma from reaching the surface [*Moran et al*., 2011].

5.2.1.2. Deflation

[44] At Sinabung and Kerinci, the inflation led to eruption associated with or followed by relatively rapid subsidence (Figure 9, stage c, case 1), while at Agung, the inflation was followed by a period of slow subsidence (Figure 9, stage c′, case 2).

[45] Coeruptive, quasi-instantaneous subsidence is expected in response to the removal of magma and gas during the eruption (elastic deformation), while posteruptive subsidence due to viscoelastic relaxation is expected with a temporal delay [e.g., *Brandsdottir and Einarsson*, 1979; *Thordarson*, 2009]. As noted earlier, subsidence at Sinabung was not only coeruptive but likely also posteruptive, possibly representing both viscoelastic deformation and cooling of the reservoir. Subsidence following Kerinci's eruption was small (4 cm) and either only coeruptive or took place in the first 7 months

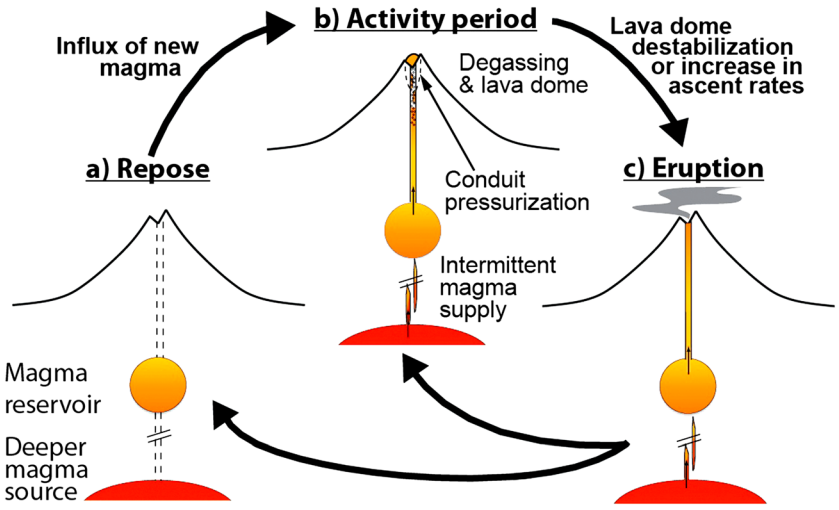

Figure 10. Cartoon for the eruptive cycle model of open volcanic systems such as Merapi, Colima, and Popocatépetl. Eruptions are not preceded by long-term edifice-wide inflation. Conduit pressurization may occur prior to eruptions, but this cannot be resolved with the low temporal resolution (46 days) of ALOS data.

following the eruption, the temporal pattern being poorly constrained. As of late 2010, Kerinci was close to its preeruption state, suggesting that only minimal magma addition or gas exsolution is necessary to bring it to its next eruption.

[46] The slow subsidence following Agung's inflation likely reflects cooling of the newly added magma (Figure 9, stage c′). This interpretation is supported by subsidence at a similar rate (~2 cm/yr) at Krafla Volcano that was explained by partial solidification and thermal contraction of a magma reservoir located around similar depths as at Agung (3 km for Krafla and 2 km for Agung) [*Sigmundsson et al*., 1997]. Cooling of Agung's reservoir could also be amplified by hydrothermal circulation due to its shallow depth. Agung's 2009–2011 deflation is less than half of the 2007–2009 inflation; thus, significant magma influx or gas exsolution is still necessary for the system to reach its critical overpressure leading to an eruption. It is likely that the next eruptions of Agung will be preceded by significant inflation.

5.2.2. Nondeforming Volcanoes: Open Systems

[47] The different activity stages at open volcanic systems are summarized in a cartoon of the eruptive cycle model in Figure 10. Similar to closed systems, when no magma is supplied from depths, the volcano is in repose (Figure 10, stage a). When magma is supplied to the shallow reservoir, the volcano enters a period of activity characterized by degassing at the vent or growth of a lava dome, reflecting the presence of a permanent or semipermanent conduit [e.g., *Wallace*, 2001] (Figure 10, stage b). In such settings, magma can rise toward the surface without pressurizing the reservoir, explaining the absence of inflation [*Albino et al.*, 2011]. Presumably, the system is permanently in a state of near eruption in which eruptions may be triggered by small intrusions into the reservoir, gradual overpressurization of the conduit, or destabilization of the lava dome (Figure 10, stage c) [*Gottsmann et al*., 2011]. The volcano either enters a period of repose or returns to its activity level preceding the eruption, depending on the magma remaining in the reservoir and on the influx from depths (Figure 10, stages a and b), and the cycle begins anew.

[48] Popocatépetl, Colima, and Merapi do not show periods of inflation prior to their numerous activity periods (in agreement with the results of *Pinel et al*. [2011] at the Mexican volcanoes). This lack of deformation cannot be explained by magma reservoirs being too deep to create detectable uplift because the volcanoes are known to have shallow reservoirs: Merapi at 2 and 8.5 km below the summit [*Ratdomopurbo and Poupinet*, 2000; *Beauducel and Cornet*, 1999] and Colima and Popocatépetl at ~4–5 km depth [*Straub et al*., 2001; *Zobin et al*., 2002]. However, these volcanoes are well known for regular eruptions, frequent open-vent degassing, and the growth of lava domes [e.g., *Taran et al*., 2001; *Delgado-Granados et al*., 2001; *Le Cloarec and Gauthier*, 2003; *Luebcke et al*., 2010], characteristics that typically define open volcanic systems [e.g., *Wallace*, 2001]. Thus, the lack of precursory inflation likely reflects that these volcanoes are open systems where limited pressurization occurs in the magma reservoirs because magma rises through already-established conduits or fractures. At Merapi, we do not detect significant deformation even during the large 2010 eruption. This suggests either that the material erupted originated from deep midcrustal reservoirs and only transited through the shallow storage system [e.g., *Grapenthin et al*., 2013b] or that the coeruptive volume changes are masked atmospheric effects and below our detection threshold. Ground-based instruments (near-field GPS, tiltmeters, and electronic distance measurement (EDM)) may allow detection of subtle coeruptive motion if not damaged by eruptive products.

[49] At Merapi, electronic distance measurement (EDM) lines detected summit inflation starting mid-September 2010 preceding the 26 October 2010 eruption [*Surono et al*., 2012]. This short-term inflation likely reflects pressurization within the conduit, supporting our interpretation of Merapi as an open volcano. However, we do not observe this inflation period in our time series because of insufficient

temporal resolution: we have one acquisition before this deformation period and one when the eruption was in progress (16 September and 1 November, respectively). SAR missions with higher temporal sampling or near-field continuous GPS may be able to detect such deformation.

6. Implications for the Potential of InSAR as a Forecast Tool for Volcanic Unrest

[50] Our results suggest that closed andesitic volcanoes have cyclic behaviors, eruptions being caused by long-term reservoir pressurization associated with edifice-wide inflation. The rate of replenishment and the volume of gas or magma drained by the eruptions likely determine the periodicity and volume of the eruptions [e.g., *Tait et al*., 1989]. In this perspective, systematic ground deformation measurements obtained by InSAR could help forecast volcanic unrest.

[51] However, there are several limitations. First, inflation is mostly detectable at volcanoes with shallow magma reservoirs. Second, open volcanic systems do not present edifice-wide long-term inflation. Third, as shown by the example of Agung, inflation does not always lead to eruption. Inflation without eruption has also been observed at several other andesitic volcanoes: Peulik, Akutan [*Lu et al*., 2007], Hualca-Hualca, Uturuncu, Lazufre [*Pritchard and Simons*, 2004], Laguna del Maule, Cordon Caulle, Cerro Hudson [*Fournier et al*., 2010], and Three Sister volcanic complex [e.g., *Riddick and Schmidt*, 2011]. To better understand how reliable inflation is as an eruption precursor, observations over multiple eruptive cycles and physics-based models are required.

[52] Many more eruptions have been documented which were not preceded by inflation (similar to Merapi, Colima, and Popocatépetl). Examples include Irruputuncu, Lascar, Nevado del Chillan, Copahue, Llaima, Villarrica, and Chaiten in Chile [*Pritchard and Simons*, 2004; *Fournier et al*., 2010]; Aracas and Ojos del Salado in Argentina [*Pritchard and Simons*, 2004]; Sabancaya and Ubinas in Peru [*Pritchard and Simons*, 2004]; Reventador in Ecuador; Nevado del Tolima and Galeras in Columbia [*Fournier et al*., 2010; *Parks et al*., 2011]; and Pavlof, Chiginagak, Shishaldin, and Veniaminof in Alaska [*Lu et al*., 2007]. Our study suggests either (1) that these volcanoes are open systems, (2) that they are closed systems and lack shallow magma reservoirs, or (3) that precursory inflation has been missed. The latter could occur because of temporal aliasing of the measurements associated with conventional InSAR (these studies did not use time series approaches). Else, a different model not requiring significant precursory inflation, such as magma filling of existing fractures, may apply [*Scandone et al*., 2007].

[53] A limitation of ALOS-type missions for identification of deformation at tropical volcanoes is the average detection threshold of ~2 cm/yr [*Ebmeier et al*., 2013] due to the atmospheric biases and to the satellite's long repeat interval (46 days). Using continuous GPS, *Cervelli et al*. [2006] detected ~1 cm of inflation prior to Augustine's 2006 eruption, in the Aleutians, but ALOS InSAR would likely have missed such small deformation related to dike propagation. Other volcanoes with precursory inflation that may have been regarded as examples of no deformation include Bromo, Indonesia in 2004 [*Abidin et al*., 2004]; Asama, Japan in 2004, 2008, and 2009 [*Takeo et al*., 2006; *Aoki et al*., 2005, 2013]; Unzendake and Kirishima, Japan in 1990–1995 and 2011, respectively [*Nishi et al*., 1999; *Nakao et al*., 2013]; and Redoubt, Aleutians in 2009 [*Grapenthin et al*., 2013a]. In the first two cases, the deformation is small because the sources are shallow (deformation related to conduit or dikes) and in the last three because the sources are deep.

[54] In summary, systematic multidecade InSAR surveys could contribute to developing better models for eruption forecasting. At closed volcanic systems, InSAR can become a powerful forecast tool if inflation is above the detection threshold. Moreover, even if the eruptive cycle model does not apply, eruptions being caused by random magma injection [*Dzurisin*, 2003], systematic ground deformation monitoring remains useful to evaluate which volcanoes of an arc are more likely to erupt in the near future. InSAR-detected deformation can also be used to deploy ground-based equipment to monitor changes in volcanic activity. Finally, when InSAR fails to detect deformation, it is likely that far-field GPS is not appropriate to evaluate volcanic unrest and other techniques should then be used to image the magma supply path (near-field GPS; EDM; strain meters; and seismic) [e.g., *Takeo et al*., 2006]. At open volcanoes, SAR amplitude images appear more useful than phase images and can be used to monitor landform changes such as deformation of lava domes, tephra distribution, or extent of volcanic flows (example of Merapi [*Pallister et al*., 2012]).

7. Conclusion

[55] A ground deformation survey of the 20 Mexican arc volcanoes revealed that none of them were inflating during 2007–2011, even the active centers Colima and Popocatépetl. Time series analysis of selected Indonesian volcanoes showed that both Sinabung and Kerinci inflated prior to their 2010 and 2009 eruptions, respectively, and deflated afterward. Agung inflated for 2 years, did not erupt, and slowly deflated afterward. No deformation was detected at Merapi despite its major eruption in 2010.

[56] We identified three types of relationships between deformation and activity: precursory inflation, inflation without eruption, and eruption without precursory deformation. Inflation occurs at closed volcanic systems as the result of pressure increase in the magma reservoirs, and an eruption follows only if the pressure reaches the critical overpressure. In contrast, open volcanic systems such as Colima, Popocatépetl, and Merapi show no significant long-term reservoir pressurization prior to eruption, suggesting that magma rises through already-established conduits. Our study suggests that InSAR can become a useful forecast tool for closed volcanic systems.

[57] **Acknowledgments.** We thank the National Aeronautics and Space Administration (NASA) for support (NNX09AK72G and NESSF11-Earth11F-0229) and the National Science Foundation (NSF) for support (EAR 0810214). The ALOS-PALSAR data are copyright of the Japanese Space Agency (JAXA) and the Japanese Ministry of Economy, Trade and Industry (METI). These data were made available by the U.S. Government Research Consortium (USGRC) through the Alaska Satellite Facility (ASF) and by the PALSAR Interferometry Consortium to Study our Evolving Land surface (PIXEL) under a cooperative research contract with the Earthquake Research Institute (ERI) of the University of Tokyo. We also thank Jeff Freymueller and an anonymous reviewer for their constructive comments.

References

Abidin, H., H. Andreas, M. Gamal, M. Hendrasto, O. K. Suganda, M. A. Purbawinata, I. Meilano, and F. Kimata (2004), The deformation of Bromo Volcano (Indonesia) as detected by GPS surveys method, *J. Global Positioning Syst.*, *3*(1–2), 16–24.

Albino, F., V. Pinel, H. Massol, and M. Collombet (2011), Conditions for detection of ground deformation induced by conduit flow and evolution, *J. Geophys. Res.*, *116*(B6), B06201, doi:10.1029/2010JB007871.

Amelung, F., S. Jonsson, H. A. Zebker, and P. Segall (2000), Widespread uplift and "trapdoor" faulting on Galapagos volcanoes observed with radar interferometry, *Nature*, *407*(6807), 993–996.

Aoki, Y., H. Watanabe, E. Koyama, J. Oikawa, and Y. Morita (2005), Ground deformation associated with the 2004–2005 unrest of Asama Volcano, Japan, *Bull. Volcanol. Soc. Jpn.*, *50*(6), 575–584.

Aoki, Y., M. Takeo, and T. Ohminato (2013), Magma pathway and its structural controls of Asama Volcano, Japan, *Geol. Soc. Spec. Publ.*, doi:10.1144/SP380.6, in press.

Baker, S., and F. Amelung (2012), Top-down inflation and deflation at the summit of Kīlauea Volcano, Hawai'i observed with InSAR, *J. Geophys. Res.*, *117*, B12406, doi:10.1029/2011JB009123.

Battaglia, M., C. Roberts, and P. Segall (1999), Magma intrusion beneath Long Valley caldera confirmed by temporal changes in gravity, *Science*, *285*(5436), 2119–2122, doi:10.1126/science.285.5436.2119.

Beauducel, F., and F. Cornet (1999), Collection and three-dimensional modeling of GPS and tilt data at Merapi volcano, Java, *J. Geophys. Res.*, *104*, 725–736.

Berardino, P., G. Fornaro, R. Lanari, and E. Sansosti (2002), A new algorithm for surface deformation monitoring based on small baseline differential SAR interferograms, *IEEE Trans. Geosci. Remote Sens.*, *40*(11), 2375–2383, doi:10.1109/TGRS.2002.803792.

Biggs, J., E. Y. Anthony, and C. J. Ebinger (2009), Multiple inflation and deflation events at Kenyan volcanoes, East African Rift, *Geology*, *37*(11), 979–982, doi:10.1130/G30133A.1.

Blake, S. (1981), Volcanism and the dynamics of open magma chamber, *Nature*, *289*, 783–785.

Blong, R. J. (1984), *Volcanic Hazards: A Sourcebook on the Effects of Eruptions*, 424 p., Academic Press Orlando, Florida.

Bower, S. M., and A. Woods (1998), On the influence of magma chambers in controlling the evolution of explosive volcanic eruptions, *J. Volcanol. Geotherm. Res.*, *86*(1), 67–78.

Brandsdottir, B., and P. Einarsson (1979), Seismic activity associated with the September 1977 deflation of the Krafla central volcano in northeastern Iceland, *J. Volcanol. Geotherm. Res.*, *6*(3), 197–212.

Cabral-Cano, E., T. H. Dixon, F. Miralles-Wilhelm, O. Diaz-Molina, O. Sanchez-Zamora, and R. E. Carande (2008), Space geodetic imaging of rapid ground subsidence in Mexico City, *Geol. Soc. Am. Bull.*, *120*(11–12), 1556–1566, doi:10.1130/B26001.1.

Casu, F., M. Manzo, and R. Lanari (2006), A quantitative assessment of the SBAS algorithm performance for surface deformation retrieval from DInSAR data, *Remote Sens. Environ.*, *102*, 195–210, doi:10.1016/j.rse.2006.01.023.

Cervelli, P. F., T. J. Fournier, J. T. Freymueller, and J. A. Power (2006), Ground deformation associated with the precursory unrest and early phases of the January 2006 eruption of Augustine Volcano, Alaska, *Geophys. Res. Lett.*, *33*, L18304, doi:10.1029/2006GL027219.

Chaussard, E., and F. Amelung (2012), Precursory inflation of shallow magma reservoirs at west Sunda volcanoes detected by InSAR, *Geophys. Res. Lett.*, *39*, L21311, doi:10.1029/2012GL053817.

Chaussard, E., F. Amelung, H. Abidin, and S.-H. Hong (2013), Sinking cities in Indonesia: ALOS PALSAR detects rapid subsidence due to groundwater and gas extraction, *Remote Sens. Environ.*, *128*, 150–161, doi:10.1016/j.rse.2012.10.015.

Colesanti, C., A. Ferretti, C. Prati, and F. Rocca (2003), Monitoring landslides and tectonic motions with the Permanent Scatterers Technique, *Eng. Geol.*, *68*, 3–14.

Davila, N., L. Capra, J. C. Gavilanes-Ruiz, N. Varley, G. Norini, and A. G. Vazquez (2007), Recent lahars at Volcán de Colima (Mexico): Drainage variation and spectral classification, *J. Volcanol. Geotherm. Res.*, *165*(3–4), 127–141, doi:10.1016/j.jvolgeores.2007.05.016.

De La Cruz-Reyna, S., I. Yokoyama, A. Martinez-Bringas, and E. Ramos (2008), Precursory seismicity of the 1994 eruption of Popocatépetl Volcano, Central Mexico, *Bull. Volcanol.*, *70*(6), 753–767.

Delgado Granados, H., L. Cárdenas González, and N. Piedad Sánchez (2001), Sulfur dioxide emissions from Popocatépetl volcano (Mexico): Case study of a high-emission rate, passively degassing erupting volcano, *J. Volcanol. Geotherm. Res.*, *108*(1), 107–120.

Denlinger, R. P., and R. P. Hoblitt (1999), Cyclic eruptive behavior of silicic volcanoes, *Geology*, *27*(5), 459–462, doi:10.1130/0091-7613(1999)027<0459:CEBOSV>2.3.CO;2.

Dragoni, M., and C. Magnanensi (1989), Displacement and stress produced by a pressurized, spherical magma chamber, surrounded by a viscoelastic shell, *Phys. Earth Planet. Inter.*, *56*, 316–328.

Dzurisin, D. (2003), A comprehensive approach to monitoring volcano deformation as a window on the eruptive cycle, *Rev. Geophys.*, *41*(1), 1001, doi:10.1029/2001RG000107.

Ebmeier, S. K., J. Biggs, T. A. Mather, and F. Amelung (2013), On the lack of InSAR observations of magmatic deformation at Central American volcanoes, *J. Geophys. Res. Solid Earth*, *118*, 2571–2585, doi:10.1002/jgrb.50195.

Emardson, T. R., M. Simons, and F. H. Webb (2003), Neutral atmospheric delay in interferometric synthetic aperture radar applications: Statistical description and mitigation, *J. Geophys. Res.*, *108*(B5), 2231, doi:10.1029/2002JB001781.

Fattahi, H., and F. Amelung (2013), DEM error correction in InSAR time-series, *IEEE Trans. Geosci. Remote Sens.*, doi:10.1109/TGRS.2012.2227761.

Ferrari, L., T. Orozco-Esquivel, V. Manea, and M. Manea (2012), The dynamic history of the Trans-Mexican Volcanic Belt and the Mexico subduction zone, *Tectonophysics*, *522-523*, 122–149, doi:10.1016/j.tecto.2011.09.018.

Fournier, T. J., M. E. Pritchard, and S. N. Riddick (2010), Duration, magnitude, and frequency of subaerial volcano deformation events: New results from Latin America using InSAR and a global synthesis, *Geochem Geophys Geosyst.*, *11*, Q01003, doi:10.1029/2009GC002558.

Froger, J., D. Remy, S. Bonvalot, and D. Legrand (2007), Two scales of inflation at Lastarria-Cordon del Azufre volcanic complex, central Andes, revealed from ASAR-ENVISAT interferometric data, *Earth Planet. Sci. Lett.*, *255*(1–2), 148–163, doi:10.1016/j.epsl.2006.12.012.

García-Palomo, A., J. Macías, and V. Garduno (2000), Miocene to Recent structural evolution of the Nevado de Toluca volcano region, Central Mexico, *Tectonophysics*, *318*, 281–302.

Gottsmann, J., S. De Angelis, N. Fournier, M. Van Camp, S. Sacks, A. T. Linde, and M. Ripepe (2011), On the geophysical fingerprint of Vulcanian explosions, *Earth Planet. Sci. Lett.*, *306*(1–2), 98–104, doi:10.1016/j.epsl.2011.03.035.

Gourmelen, N., F. Amelung, and R. Lanari (2010), Interferometric synthetic aperture radar–GPS integration: Interseismic strain accumulation across the Hunter Mountain fault in the eastern California shear zone, *J. Geophys. Res.*, *115*, B09408, doi:10.1029/2009JB007064.

Grapenthin, R., J. T. Freymueller, and A. M. Kaufman (2013a), Geodetic observations during the 2009 eruption of Redoubt Volcano, Alaska, *J. Volcanol. Geotherm. Res.*, doi:10.1016/j.jvolgeores.2012.04.021, in press.

Grapenthin, R., J. T. Freymueller, and S. S. Serovetnikov (2013b), Surface deformation of Bezymianny Volcano, Kamchatka, recorded by GPS: The eruptions from 2005 to 2010 and long-term, long-wavelength subsidence, *J. Volcanol. Geotherm. Res.*, *1–17*, doi:10.1016/j.jvolgeores.2012.11.012, in press.

Gudmundsson, A. (2012), Magma chambers: Formation, local stresses, excess pressures, and compartments, *J. Volcanol. Geotherm. Res.*, *237-238*(C), 19–41, doi:10.1016/j.jvolgeores.2012.05.015.

Hansen, J. E., W. C. Wang, and A. A. Lacis (1978), Mount Agung eruption provides test of a global climatic perturbation, *Science*, *199*(4333), 1065–1068.

Hughes, G. R., and G. A. Mahood (2011), Silicic calderas in arc settings: Characteristics, distribution, and tectonic controls, *Geol. Soc. Am. Bull.*, *123*(7–8), 1577–1595, doi:10.1130/B30232.1.

James, M. R., and N. Varley (2012), Identification of structural controls in an active lava dome with high resolution DEMs: Volcán de Colima, Mexico, *Geophys. Res. Lett.*, *39*, L22303, doi:10.1029/2012GL054245.

Jellinek, A. M., and D. J. DePaolo (2003), A model for the origin of large silicic magma chambers: Precursors of caldera-forming eruptions, *Bull. Volcanol.*, *65*(5), 363–381, doi:10.1007/s00445-003-0277-y.

Jolivet, R., R. Grandin, C. Lasserre, M. P. Doin, and G. Peltzer (2011), Systematic InSAR tropospheric phase delay corrections from global meteorological reanalysis data, *Geophys. Res. Lett.*, *38*, L17311. doi:10.1029/2011GL048757.

Lanari, R., O. Mora, M. Manunta, J. J. Mallorqui, P. Berardino, and E. Sansosti (2004), A small-baseline approach for investigating deformations on full-resolution differential SAR interferograms, *IEEE Trans. Geosci. Remote Sens.*, *42*, 1377–1386.

Le Cloarec, M.-F., and P. J. Gauthier (2003), Merapi Volcano, Central Java, Indonesia: A case study of radionuclide behavior in volcanic gases and its implications for magma dynamics at andesitic volcanoes, *J. Geophys. Res.*, *108*(B5), 2243, doi:10.1029/2001JB001709.

Lu, Z., C. W. Wicks Jr., D. Dzurisin, J. A. Power, S. C. Moran, and W. Thatcher (2002), Magmatic inflation at a dormant stratovolcano: 1996–1998 activity at Mount Peulik volcano, Alaska, revealed by satellite radar interferometry, *J. Geophys. Res.*, *107*(B7), 2134, doi:10.1029/2001JB000471.

Lu, Z., T. Masterlark, D. Dzurisin, R. Rykhus, and C. W. Wicks Jr. (2003), Magma supply dynamics at Westdahl volcano, Alaska, modeled from satellite radar interferometry, *J. Geophys. Res.*, *108*(B7), 2354 doi:10.1029/2002JB002311.

Lu, Z., T. Masterlark, and D. Dzurisin (2005), Interferometric synthetic aperture radar study of Okmok volcano, Alaska, 1992–2003: Magma supply dynamics and postemplacement lava flow deformation. *J. Geophys. Res.*, *110*, B02403, doi:10.1029/2004JB003148.

Lu, Z., D. Dzurisin, C. W. Wicks Jr., J. A. Power, J. Kwoun, and R. Rykhus (2007), Diverse deformation patterns of Aleutian volcanoes from satellite interferometric synthetic aperture radar (InSAR). (J. Eichelberger, E. Gordeev, P. E. Izbekov, M. Kasahara, & J. Lees, Eds.). Volcanism and Subduction, *AGU Monogr. Ser.*, *172*, 249–261, doi:10.1029/172GM18.

Luebcke, P., J. Zielcke, L. Vogel, C. Kern, N. Bobrowski, and U. Platt (2010), Observing the plume of Popocatépetl with a novel SO2-Camera. AGU Fall Meeting 2010, abstract #NH43A-1495.

Massonnet, D., M. Rossi, C. Carmona, F. Adragna, G. Peltzer, K. L. Feigl, and T. Rabaute (1993), The displacement field of the Landers earthquake mapped by radar interferometry, *Nature*, *364*, 138–142.

McCaffrey, R. (2009), The tectonic framework of the Sumatran subduction zone, *Annu. Rev. Earth Planet. Sci.*, *37*(1), 345–366, doi:10.1146/annurev.earth.031208.100212.

Moran, S. C., C. Newhall, and D. C. Roman (2011), Failed magmatic eruptions: Late-stage cessation of magma ascent, *Bull. Volcanol.*, *73*(2), 115–122, doi:10.1007/s00445-010-0444-x.

Nakao, S., Y. Morita, H. Yakiwara, J. Oikawa, H. Ueda, H. Takahashi, Y. Ohta, T. Matsushima, and M. Iguchi (2013), Volume change of the magma reservoir relating to the 2011 Kirishima Shinmoe-dake eruption —Charging, discharging and recharging process inferred from GPS measurements, *Earth, Planets Space*, *65*, 505–515, doi:10.5047/eps.2013.05.017.

Newhall, C. G. (2007), Volcanology 101 for seismologists, in *Treatise on Geophysics*, edited by G. Schubert and H. Kanamori, *4.12*, pp. 351–388, Elsevier, Amsterdam, The Netherlands, doi:10.1016/B978-044452748-6.00072-9.

Nishi, K., H. Ono, and H. Mori (1999), Global positioning system measurements of ground deformation caused by magma intrusion and lava discharge: The 1990–1995 eruption at Unzendake volcano, Kyushu, Japan, *J. Volcanol. Geotherm. Res.*, *89*, 23–34.

Nishimura, T. (2009), Ground deformation caused by magma ascent in an open conduit, *J. Volcanol. Geotherm. Res.*, *187*(3–4), 178–192, doi:10.1016/j.jvolgeores.2009.09.001.

Osmanoglu, B., T. H. Dixon, S. Wdowinski, E. Cabral-Cano, and Y. Jiang (2011), Mexico City subsidence observed with persistent scatterer InSAR, *Int. J. Appl. Earth Observations Geoinf.*, *13*(1), 1–12, doi:10.1016/j.jag.2010.05.009.

Pallister, J. S., D. J. Schneider, J. P. Griswold, R. H. Keeler, W. C. Burton, C. Noyles, and C. G. Newhall (2012), Merapi 2010 eruption—Chronology and extrusion rates monitored with satellite radar and used in eruption forecasting, *J. Volcanol. Geotherm. Res.*, *1–9*, doi:10.1016/j.jvolgeores.2012.07.012.

Parks, M. M., J. Biggs, T. A. Mather, D. M. Pyle, F. Amelung, M. L. Monsalve, and L. N. Medina (2011), Co-eruptive subsidence at Galeras identified during an InSAR survey of Colombian volcanoes (2006–2009), *J. Volcanol. Geotherm. Res.*, *202*(3–4), 228–240, doi:10.1016/j.jvolgeores.2011.02.007.

Pinel, V., C. Jaupart, and F. Albino (2010), On the relationship between cycles of eruptive activity and growth of a volcanic edifice, *J. Volcanol. Geotherm. Res.*, *194*(4), 150–164, doi:10.1016/j.jvolgeores.2010.05.006.

Pinel, V., A. Hooper, L. Cruz-Reyna, S. De, G. Reyes-Davila, M. P. Doin, and P. Bascou (2011), The challenging retrieval of the displacement field from InSAR data for andesitic stratovolcanoes: Case study of Popocatépetl and Colima Volcano, Mexico, *J. Volcanol. Geotherm. Res.*, *200*(1–2), 49–61, doi:10.1016/j.jvolgeores.2010.12.002.

Pritchard, M. E., and M. Simons (2004), An InSAR-based survey of volcanic deformation in the southern Andes, *Geophys. Res. Lett.*, *31*, L15610, doi:10.1029/2004GL020545.

Ramírez-Herrera, M. T., and J. Urrutia-Fucugauchi (1999), Morphotectonic zones along the coast of the Pacific continental margin, southern Mexico, *Geomorphologie*, *28*(3), 237–250.

Ratdomopurbo, A., and G. Poupinet (2000), An overview of the seismicity of Merapi volcano (Java, Indonesia), 1983–1994, *J. Volcanol. Geotherm. Res.*, *100*, 193–214.

Riddick, S. N., and D. A. Schmidt (2011), Time-dependent changes in volcanic inflation rate near Three Sisters, Oregon, revealed by InSAR, *Geochem Geophys Geosyst.*, *12*, Q12005, doi:10.1029/2011GC003826.

Rosen, P. A., S. Hensley, G. Peltzer, and M. Simons (2004), Updated repeat orbit interferometry package released, *Eos Trans. AGU*, *85*(5), 47, doi:10.1029/2004EO050004.

Scandone, R., K. V. Cashman, and S. D. Malone (2007), Magma supply, magma ascent and the style of volcanic eruptions, *Earth Planet. Sci. Lett.*, *253*(3–4), 513–529, doi:10.1016/j.epsl.2006.11.016.

Self, S., and M. R. Rampino (2012), The 1963–1964 eruption of Agung volcano (Bali, Indonesia), *Bull. Volcanol.*, *74*(6), 1521–1536, doi:10.1007/s00445-012-0615-z.

Sigmundsson, F., H. Vadon, and D. Massonnet (1997), Readjustment of the Krafla spreading segment to crustal rifting measured by satellite radar interferometry, *Geophys. Res. Lett.*, *24*, 1843–1846.

Simkin, T., and L. Siebert (2002), Global Volcanism Program. Smithsonian Institution, Global Volcanism Program Digital Information Series, GVP-5. http://www.volcano.si.edu/education/questions/.

Straub, S., and A. L. Martin-Del Pozzo (2001), The significance of phenocryst diversity in tephra from recent eruptions at Popocatépetl volcano (central Mexico), *Contrib. Mineral. Petrol.*, *140*(4), 487–510.

Surono, J. P., et al. (2012), The 2010 explosive eruption of Java's Merapi volcano—A '100-year' event, *J. Volcanol. Geotherm. Res.*, *241-242*(C), 121–135, doi:10.1016/j.jvolgeores.2012.06.018.

Tait, S., C. Jaupart, and S. Vergniolle (1989), Pressure, gas content and eruption periodicity of a shallow, crystallizing magma chamber, *Earth Planet. Sci. Lett.*, *92*(1), 107–123.

Takeo, M., Aoki, Y., Ohminato, T., and Yamamoto, M. (2006), Magma supply path beneath Mt. Asama volcano Japan, *Geophys. Res. Lett.*, *33*, L15310, doi:10.1029/2006GL026247.

Taran, Y. A., A. Bernard, J. C. Gavilanes, E. Lunezheva, A. Cortes, and M. A. Armienta (2001), Chemistry and mineralogy of high-temperature gas discharges from Colima volcano, Mexico. Implications for magmatic gas–atmosphere interaction, *J. Volcanol. Geotherm. Res.*, *108*(1), 245–264.

Thordarson, T. (2009), Studies in Volcanology: The Legacy of George Walker (No. 2). Geological Society Publishing House.

Tizzani, P., P. Berardino, F. Casu, P. Euillades, M. Manzo, G. P. Ricciardi, G. Zeni, and R. Lanari (2007), Surface deformation of Long Valley Caldera and Mono Basin, California, investigated with the SBAS-InSAR approach, *Remote Sens. Environ.*, *108*(3), 277–289, doi:10.1016/j.rse.2006.11.015.

Toombs, A., and G. Wadge (2012), Co-eruptive and inter-eruptive surface deformation measured by satellite radar interferometry at Nyamuragira volcano, D.R. Congo, 1996 to 2010, *J. Volcanol. Geotherm. Res.*, *245–246*, 98–122, doi:10.1016/j.jvolgeores.2012.07.005.

Vazquez, J. A., and M. R. Reid (2004), Probing the accumulation history of the voluminous Toba magma, *Science*, *305*, 991–994.

Voight, B., et al. (1999), Magma flow instability and cyclic activity at Soufrière Hills volcano, Montserrat, British West Indies, *Science*, *283*(5405), 1138–1142, doi:10.1126/science.283.5405.1138.

Wallace, P. J. (2001), Volcanic SO_2 emissions and the abundance and distribution of exsolved gas in magma bodies, *J. Volcanol. Geotherm. Res.*, *108*(1–4), 85–106, doi:10.1016/S0377-0273(00)00279-1.

White, S. M., J. A. Crisp, and F. J. Spera (2006), Long-term volumetric eruption rates and magma budgets, *Geochem Geophys Geosyst.*, *7*(3), Q03010, doi:10.1029/2005GC001002.

Wicks, C. W. Jr., J. C. de la Llera, L. E. Lara, and J. Lowenstern (2011), The role of dyking and fault control in the rapid onset of eruption at Chaitén volcano, Chile, *Nature*, *478*(7369), 374–377, doi:10.1038/nature10541.

Zebker, H. A., P. A. Rosen, and S. Hensley (1997), Atmospheric effects in interferometric synthetic aperture radar surface deformation and topographic maps, *J. Geophys. Res.*, *102*, 7547–7563.

Zellmer, G. F., C. Annen, B. L. A. Charlier, R. M. M. George, S. P. Turner, and C. J. Hawkesworth (2005), Magma evolution and ascent at volcanic arcs: Constraining petrogenetic processes through rates and chronologies, *J. Volcanol. Geotherm. Res.*, *140*(1), 171–191, doi:10.1016/j.jvolgeores.2004.07.020.

Zobin, V., et al. (2002), Overview of the 1997–2000 activity of Volcan de Colima, Mexico, *J. Volcanol. Geotherm. Res.*, *117*, 1–19.

Zobin, V. M., C. Navarro, G. Reyes-Dávila, J. Orozco, M. Bretón, A. Tellez, G. Reyes-Alfaro, and H. Vázquez (2006), The methodology of quantification of volcanic explosions from broad-band seismic signals and its application to the 2004–2005 explosions at Volcán de Colima, Mexico, *Geophys. J. Int.*, *167*(1), 467–478, doi:10.1111/j.1365-246X.2006.03108.x.

Zobin, V. M., I. Plascencia, G. Reyes, and C. Navarro (2009), The characteristics of seismic signals produced by lahars and pyroclastic flows: Volcán de Colima, Mexico, *J. Volcanol. Geotherm. Res.*, *179*(1–2), 157–167, doi:10.1016/j.jvolgeores.2008.11.001.